THE JOURNAL OF PHYSICAL CHEMISTRY A

Article

pubs.acs.org/JPCA

Spectroscopic Distinctions between Two Types of Ce^{3+} Ions in X2-Y_2SiO_5: A Theoretical Investigation

Jun Wen,*[,†] Chang-Kui Duan,[‡] Lixin Ning,*[,§] Yucheng Huang,[§] Shengbao Zhan,[†] Jie Zhang,[†] and Min Yin[‡]

[†]School of Physics and Electronic Engineering, Anqing Normal University, Anqing 246011, People's Republic of China

[‡]Department of Physics, University of Science and Technology of China, Hefei 230026, People's Republic of China

[§]Center for Nano Science and Technology, Department of Physics, Anhui Normal University, Wuhu 241000, People's Republic of China

ABSTRACT: The Ce^{3+} ions occupying the two crystallographically distinct Y^{3+} sites both with C_1 point group symmetry in the X2-Y_2SiO_5 (X2-YSO) crystal are discriminated by their spectroscopic properties calculated with *ab initio* approaches and phenomenological model analyses. Density functional theory (DFT) calculations with the supercell approach are performed to obtain the local structures of Ce^{3+}, based on which the wave function-based embedded cluster calculations at the CASSCF/CASPT2 level are carried out to derive the 4f → 5d transition energies. From the *ab initio* calculated energy levels and wave functions, the crystal-field parameters (CFPs) and the anisotropic *g*-factor tensors of Ce^{3+} are extracted. The theoretical results agree well with available experimental data. The structural and spectroscopic properties for the two types of Ce^{3+} ions in X2-YSO are thus distinguished in terms of the calculated local atomic structures, 4f → 5d transition energies, and spectral parameters.

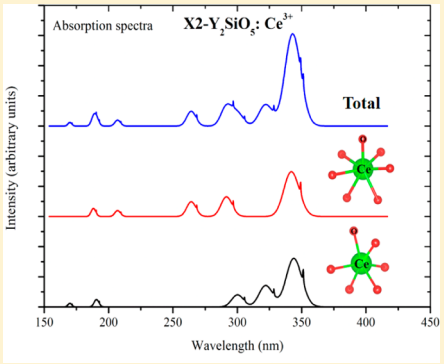

1. INTRODUCTION

Yttrium orthosilicate (Y_2SiO_5, YSO) is an important host crystal for doping with transition-metal and lanthanide ions, due to their wide applications in lighting and displays, scintillators, and solid-state lasers.[1−4] Recently, the application of lanthanide-doped YSO in quantum information has been extensively explored,[5−10] for which the knowledge of the hyperfine structures of the ground and excited states of the dopant ion is indispensable. Some experimental techniques, such as electron paramagnetic resonance (EPR) and spectral hole-burning measurements,[7−10] have been employed to investigate these hyperfine structures and the relative strengths of the characteristic optical transitions. There are two crystallographic forms for YSO, namely, X1- and X2-YSO, corresponding to the low and high temperature phases, respectively. In each phase, two crystallographically different Y^{3+} sites exist, with coordination numbers (CNs) of seven and nine in X1-YSO, and six and seven in X2-YSO, which will be referred to as Y1 and Y2 sites, respectively (see Figure 1).

Ce^{3+} ion in YSO may serve as a readout ion to probe the single-ion qubit state for the quantum computing scheme,[11,12] due to its electric dipole allowed 5d → 4f luminescence with a fast decay time of several tens of nanoseconds. The 5d excited states of Ce^{3+} exhibit a stronger coupling to the local crystalline environment than the 4f ground states, and thus the 5d → 4f transitions can be easily affected by its coordination structure.[13−15] The dopant Ce^{3+} displays a higher luminescence intensity in X2-YSO than in X1-YSO, due to a smaller number of nonradiative relaxation processes.[16] Experimental excitation and emission spectral measurements revealed the presence of two types of Ce^{3+} centers in X2-YSO.[17] Although it is supposed to be due to the Ce^{3+} occupying the two distinct Y^{3+} sites, a definitive characterization of the spectra in association with the local structures is still not available. Since such information is essential to understand the optical properties of Ce-doped X2-YSO, we have carried out *ab initio* calculations to obtain the local structures and 4f → 5d transition energies of Ce^{3+} at the two different Y^{3+} sites in X2-YSO. By comparing the calculated transition energies with experimental excitation spectra, the two

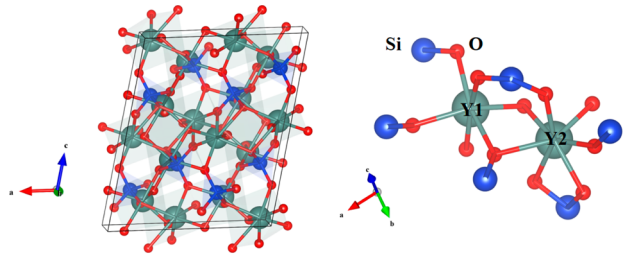

Figure 1. Schematic representations of local atomic structures around the two types of yttrium (Y1 and Y2) sites along with the unit cell of X2-YSO.

Received: May 22, 2014
Revised: June 21, 2014
Published: June 21, 2014

   dx.doi.org/10.1021/jp5050207 | *J. Phys. Chem. A* 2014, 118, 4988−4994

types of Ce^{3+} centers are identified in relation to the coordination structures of the dopant sites.

Using the *ab initio* calculated energy levels and wave functions for the $4f^1$ and $5d^1$ configurations of Ce^{3+}, we have also calculated the 4f and 5d crystal-field parameters (CFPs) with an effective operator approach,[18−21] which may provide a basis for the analysis of energy levels for other lanthanide ions in X2-YSO. Moreover, with the derived 4f CFPs, we have constructed an effective Hamiltonian that includes the interaction of 4f electrons with an external magnetic field. Based on this Hamiltonian, the anisotropic *g*-factor tensors of Ce^{3+} have been extracted and compared with the data derived from experimental EPR spectra. The main purpose of this work is to demonstrate the ability of a combined *ab initio* and phenomenological approach to elucidate spectroscopic properties of Ce^{3+} in low-symmetry systems. The rest of this paper is organized as follows. Section 2 describes the methodology adopted in this work. In section 3, the results and discussion of structural properties, 4f → 5d transitions, spectral parameters, and spectroscopic distinctions of the two types of Ce^{3+} are presented. Finally, our conclusions are given in section 4.

2. METHODOLOGY

2.1. DFT Calculations of Local Structures. The local structure of Ce^{3+} located at the six- or seven-coordinated Y^{3+} site in X2-YSO was calculated by using the density functional theory (DFT) method with the PBE functional,[22] as implemented in the VASP package.[23,24] A 1 × 2 × 1 supercell containing 128 atoms was chosen to model the Ce-doped X2-YSO crystal, in which one of 16 Y1 or Y2 atoms was replaced by a Ce atom, corresponding to a doping concentration of 3.125%. The Ce $5s^25p^64f^15d^16s^2$, Y $4s^24p^64d^15s^2$, Si $3s^23p^2$, and O $2s^22p^4$ electrons were treated explicitly, and their interactions with the cores were described by the projected augmented wave (PAW) method.[25] The supercell structures were fully optimized using the conjugate gradient technique until the energy change was less than 10^{-6} eV and the Hellmann−Feynman forces on atoms were less than 0.01 eV/Å. The plane-wave cutoff energy was set to 550 eV, and one *k*-point Γ for sampling the Brillouin zone was used.

2.2. CASSCF/CASPT2 Calculations of Ce^{3+} 4f → 5d Transition Energies. Based on the DFT-optimized supercell structures, two Ce-centered clusters, $(Ce_{Y1}O_6Si_4)^{7+}$ and $(Ce_{Y2}O_7Si_4)^{5+}$, containing the atoms in the first- and second-coordination shells, were constructed. The lattice environments of the clusters were simulated by embedding *ab initio* model potentials (AIMPs)[26] with a sphere of radius 10.0 Å and point charges with a sphere of radius 30.0 Å located at the lattice sites. For the two embedded clusters, the wave function-based CASSCF/CASPT2 calculations[27−32] were performed to obtain the $4f^1$ and $5d^1$ energy levels as well as the corresponding wave functions with the program MOLCAS.[33] In the CASSCF calculations, the energies and wave functions were obtained by minimizing the average energy of the 13 states, generated by occupying the single unpaired electron on one of the 13 molecular orbitals with main characters of 4f, 5d, and 6s of Ce^{3+} ion. In the CASPT2 calculations, the dynamic correlation effects of Ce^{3+} 5s, 5p, 4f, and 5d and O^{2-} 2s, and 2p electrons were taken into account by using the CASSCF wave functions. With the CASSCF wave functions and CASPT2 energies, the spin−orbit coupling (SOC) effect was considered by adopting the restricted-active-space state-interaction spin−orbit (RASSI-SO) method.[34] A relativistic effective core potential ([Kr] core) with a (14s10p10d8f3g)/[6s5p6d4f1g] Gaussian valence basis set from ref 35 was used for Ce, a [He] core effective core potential with a (5s6p1d)/[2s4p1d] valence basis set from ref 36 was employed for O, and a [Ne] core effective potential and a (7s6p1d)/(2s3p1d) valence basis set from ref 36 was adopted for Si. These basis sets were further augmented by the respective auxiliary spin−orbit basis sets for a proper description of the inner core region in the spin−orbit calculations.

2.3. Phenomenological Model Analyses of $4f^1$ Energy Levels of Ce^{3+} Ion. The phenomenological model analyses of energy levels of lanthanide ions are usually performed by using an effective Hamiltonian, which acts within the $4f^N$ or $4f^{N-1}5d$ configuration.[37] The effective Hamiltonian comprises two different parts. One part is the atomic interaction of the 4f or 5d electrons, and the other is the CF interaction of the 4f or 5d electrons with their environments. For the $4f^1$ ground-state configuration of Ce^{3+}, the atomic part includes only the spin−orbit interaction, which can be expressed as $H_{SO} = \xi_{4f}\mathbf{A}_{SO}$, where ξ_{4f} is the spin−orbit parameter usually determined empirically, and $\mathbf{A}_{SO}$ is an operator representing the angular part of the interaction. The CF interaction can be written as[37]

$$H_{CF} = \sum_{k,q} B_q^k C_q^k \tag{1}$$

where B_q^k are the CFPs and C_q^k are the spherical tensor operators. For the $4f^N$ configuration, the summation is over k = 2, 4, and 6 and $|q| \leq k$. The number of nonzero B_q^k is determined by the site symmetry of the lanthanide ion, and their values could in principle be obtained by fitting to experimental energy-level data. For Ce^{3+} in X2-YSO, the site symmetries of the two dopant sites are C_1, and a total of 27 or 14 nonzero B_q^k parameters would be required for the $4f^1$ or $5d^1$ configuration, for which, however, only a maximum of seven or five energy levels exists. As such, in this work the CFPs for Ce^{3+} in X2-YSO are derived from the *ab initio* calculated energy levels and wave functions. The details for the extraction of CFPs of lanthanide ions from *ab initio* calculations may be found in refs 18−20.

The spin Hamiltonian of the system in the presence of an external magnetic field may be expressed as

$$H_Z = g_J\mu_B\mathbf{J}\cdot\mathbf{B} \tag{2}$$

where the hyperfine and nuclear Zeeman interactions have been ignored, g_J is the effective Lande *g* factor, μ_B is the Bohr magneton, **J** is the total angular momentum, and **B** is the external magnetic field. In an external magnetic field, the Kramers degeneracy of CF energy levels is completely removed.

2.4. Extraction of the g Tensors of Ce^{3+} Sites. On the basis of the *ab initio* calculated CFPs, the method[38] of extracting the **g**-factors of Ce^{3+} from diagonalization of the whole energy matrix of the effective Hamiltonian can be extended to the cases with low site symmetries. According to ref 39, the relationship between the measurable matrix $\mathbf{g}\cdot\mathbf{g}^T$ (the superscript T denotes the matrix transpose operation) and the $g^2(\mathbf{n})$ factor (corresponding to the external magnetic field along an arbitrary direction **n**) is expressed as

$$g^2(\mathbf{n}) = \mathbf{n}^T\cdot(\mathbf{g}\cdot\mathbf{g}^T)\cdot\mathbf{n} \tag{3}$$

Considering the external field along a certain direction, eq 3 is then transformed to

dx.doi.org/10.1021/jp5050207 | J. Phys. Chem. A 2014, 118, 4988−4994

$$g^2(\mathbf{n}_\alpha) = (\mathbf{g}\cdot\mathbf{g}^T)_{\alpha\alpha} \quad (4)$$

and

$$g^2(\mathbf{n}_{\alpha\pm\beta}) = \frac{1}{2}[(\mathbf{g}\cdot\mathbf{g}^T)_{\alpha\alpha} + (\mathbf{g}\cdot\mathbf{g}^T)_{\beta\beta} \pm 2(\mathbf{g}\cdot\mathbf{g}^T)_{\alpha\beta}] \quad (5)$$

where $\mathbf{n}_\alpha$ and $\mathbf{n}_\beta$ denote the different basis vectors of the Cartesian coordinate system, $\mathbf{n}_{\alpha+\beta}$ and $\mathbf{n}_{\alpha-\beta}$ are the unit vectors in the directions of $\mathbf{n}_\alpha + \mathbf{n}_\beta$ and $\mathbf{n}_\alpha - \mathbf{n}_\beta$, respectively. Consequently, the off-diagonal component of $\mathbf{g}\cdot\mathbf{g}^T$ can be expressed as

$$(\mathbf{g}\cdot\mathbf{g}^T)_{\alpha\beta} = \frac{2g^2(\mathbf{n}_{\alpha+\beta}) - g^2(\mathbf{n}_\alpha) - g^2(\mathbf{n}_\beta)}{2} = \frac{g^2(\mathbf{n}_{\alpha+\beta}) - g^2(\mathbf{n}_{\alpha-\beta})}{2} \quad (6)$$

From eqs 4 and 6, the matrix elements of $\mathbf{g}\cdot\mathbf{g}^T$ can be determined once the $g^2(\mathbf{n})$ factors are calculated. The $\mathbf{g}\cdot\mathbf{g}^T$ matrix is always symmetric, and hence only six independent matrix elements need to be determined.

Moreover, the splitting value ΔE of the ground-state Kramers doublet of Ce^{3+} under an external magnetic field can be determined by diagonalizing the matrix of the effective Hamiltonian, which is constructed by using the *ab initio* calculated 4f CFPs (from the CASPT2-calculated energies), the empirically determined 4f spin−orbit parameter (614.9 cm^{-1} from ref 40), and the external magnetic field with certain magnitude and direction. As is well-known, this splitting value can also be expressed as $\Delta E = E_+ - E_- = g\mu_B B$, where E_+ and E_- ($E_\pm = \pm(1/2)g\mu_B B$) are the eigenvalues of the spin Hamiltonian. The $g^2(\mathbf{n})$ factor is thus derived

$$g^2(\mathbf{n}) = \left[\frac{\Delta E(\mathbf{n})}{\mu_B B(\mathbf{n})}\right]^2 \quad (7)$$

from which the matrix $\mathbf{g}\cdot\mathbf{g}^T$ and subsequently the $\mathbf{g}$-factor tensor of Ce^{3+} site can be derived.

3. RESULTS AND DISCUSSION

The DFT-optimized lattice parameters of pure X2-YSO are listed in Table 1. It can be seen that the calculated lattice parameters are slightly larger than the experimental ones by 1−2%. The discrepancies can be traced to the inherent shortcomings of the DFT-PBE functional. In Table 2, we list the optimized Ce^{3+}−O^{2-} bond lengths for the two types of Ce^{3+} sites in X2-YSO, together with those of Y^{3+}−O^{2-} in the pure crystal for comparison. It is shown that the Ce^{3+}−O^{2-} bond length is larger than that of the corresponding Y^{3+}−O^{2-} bond. The increments of bond lengths are in the ranges of 0.072−0.105 Å and 0.040−0.113 Å for Ce^{3+} at the six-coordinated Y1 site and the seven-coordinated Y2 site, respectively, which is qualitatively consistent with the larger ionic radius of Ce^{3+} than Y^{3+} with the same CN.[42] Moreover, the results of DFT total energies of the Ce-doped supercells indicate that the dopant Ce^{3+} prefers to occupy the larger Y2 site than the smaller Y1 site by 219 meV. This site preference is in agreement with the observation from EPR spectroscopic measurements,[43] which show that the relative populations of the two types of Ce^{3+} ions are found to be 95% (CN = 7) and 5% (CN = 6), respectively.

Table 1. Calculated and Experimental Lattice Parameters for X2-YSO

method	*a* (Å)	*b* (Å)	*c* (Å)	*β* (deg)
DFT-PBE[a]	10.551	6.832	12.639	102.88
experiment[b]	10.410	6.721	12.490	102.65

[a]In our calculations, the included angle between our chosen *X* axis and the basis vector $\mathbf{n}_a$ of unit cell (ref 41) is 12.65°; the *Y* and *Z* axes are parallel to the basis vectors $\mathbf{n}_b$ and $\mathbf{n}_c$ of the unit cell (ref 41), respectively. [b]Reference 41.

Table 2. DFT-Optimized Y^{3+}−O^{2-} and Ce^{3+}−O^{2-} Bond Lengths (in Å) in X2-YSO

site 1[a] (CN = 6)	M = Y1	M = Ce_{Y1}
M−O1	2.229	2.301 (+0.072)
M−O2	2.296	2.401 (+0.105)
M−O3	2.300	2.394 (+0.094)
M−O4	2.301	2.403 (+0.102)
M−O5	2.302	2.401 (+0.099)
M−O6	2.322	2.404 (+0.082)
site 2[b] (CN = 7)	M = Y2	M = Ce_{Y2}
M−O1	2.223	2.308 (+0.085)
M−O2	2.309	2.409 (+0.100)
M−O3	2.337	2.425 (+0.088)
M−O4	2.367	2.424 (+0.057)
M−O5	2.399	2.499 (+0.100)
M−O6	2.401	2.514 (+0.113)
M−O7	2.697	2.737 (+0.040)

[a]Ce^{3+} ion at site 1 replaces the Y^{3+} ion with the optimized and experimental (ref 41) internal parameters (0.431, 0.756, 0.463) and (0.429, 0.757, 0.463), respectively. [b]Ce^{3+} ion at site 2 replaces the Y^{3+} ion with the optimized and experimental (ref 41) internal parameters (0.305, 0.118, 0.643) and (0.306, 0.122, 0.641), respectively.

The wave function based CASSCF/CASPT2 calculations were performed on the Ce-centered embedded clusters, which were constructed from the DFT-optimized supercell geometries, to obtain the $4f^1$ and $5d^1$ energy levels of Ce^{3+}. The results are listed in Table 3. As expected, the inclusion of the SOC effect changes dramatically the energy-level structure of the $4f^1$ configuration. For the $5d^1$ configuration, the SOC effect is much less pronounced, and it only raises the $5d^1$ energy levels uniformly by around 1000 cm^{-1}. The results in the table also show that the $4f^1$ and $5d^1$ CF splittings of Ce_{Y1}^{3+} are larger by ∼550 and ∼6000 cm^{-1} than those of Ce_{Y2}^{3+}, consistent with the fact that a smaller site usually produces a larger CF splitting.[45] However, the barycenter energies of the $5d^1$ configuration for the two types of Ce^{3+} are similar, with the value for Ce_{Y1}^{3+} slightly larger than that for Ce_{Y2}^{3+} (by 500−600 cm^{-1}), and thus the site-size effect on the $5d^1$ barycenter energy is not so important as that on the $5d^1$ CF splitting, in agreement with the observation made by Dorenbos.[45] A further detailed comparison of the calculated energy levels with experimental results will be presented later.

On the basis of the wave functions from CASSCF calculations and the energy levels from CASSCF or CASPT2 calculations, the 4f and 5d CFPs for Ce^{3+} at the Y1 and Y2 sites were extracted, using an effective operator method described in refs 18−20. The results are listed in Table 4. It is shown that the 4f and 5d scalar CF strengths (*S*, as expressed in the footnotes of the table) of Ce_{Y1}^{3+} are much larger than those of Ce_{Y2}^{3+}, indicating stronger 4f and 5d CF interactions present at the former site, consistent with the previous analysis based on

dx.doi.org/10.1021/jp5050207 | J. Phys. Chem. A 2014, 118, 4988−4994

Table 3. Calculated CASPT2 Energies without and with the Spin-Orbit Coupling (SOC) Effect for the $4f^1$ and $5d^1$ Levels (in cm^{-1}) of Ce^{3+} Ions in X2-YSO, along with the Available Experimental Data[a]

	site 1 (CN = 6, $(Ce_{Y1}O_6Si_4)^{7+}$)			site 2 (CN = 7, $(Ce_{Y2}O_7Si_4)^{5+}$)			LSO Ce^{3+}, CN = 6		LSO Ce^{3+}, CN = 7	
levels[b]	without SOC	with SOC	exptl[c]	without SOC	with SOC	exptl[c]	calcd[d]	exptl[d]	calcd[d]	exptl[d]
$4f_1$	0	0		0	0		0		0	
$4f_2$	203	483		180	228		430		373	
$4f_3$	569	1205		402	649		1116		676	
$4f_4$	885	2177		444	2209		2173		2227	
$4f_5$	1191	2792		468	2392		2648		2447	
$4f_6$	1817	3275		750	2615		3252		2742	
$4f_7$	2593	4099		1965	3543		3978		3480	
$5d_1$	27748	28470		27565	28498		28603	27139	28872	28070
$5d_2$	29411	30396	31250	32557	33555	33333	31257	30700	34905	33884
$5d_3$	31582	32657		36028	37090	38462	33518		38027	38017
$5d_4$	50804	51834	52632	46391	47567	47619	51966		47812	
$5d_5$	57191	58217		51244	52381	55556	58082		52592	
ΔE_{5d}	29443	29747		23679	23883		29479		23720	
$\bar{E}_{5d}$	39347	40315		38757	39818		40685		40442	

[a]The experimental and calculated data of Ce^{3+} ions in LSO are also listed for comparison. [b]ΔE_{5d}, the CF splitting of $5d^1$ energy levels; $\bar{E}_{5d}$, the centroid of $5d^1$ energy levels. [c]The experimentally determined $5d^1$ energy levels of Ce^{3+} ions in X2-YSO from the excitation peak energies in ref 17. [d]The experimentally determined and *ab initio* calculated $5d^1$ energy levels of Ce^{3+} ions in LSO from ref 44.

Table 4. Calculated CFPs B_q^k with $q \geq 0$ (in cm^{-1}) for Ce^{3+} Ions in X2-YSO

		site 1 (CN = 6, $(Ce_{Y1}O_6Si_4)^{7+}$)				site 2 (CN = 7, $(Ce_{Y2}O_7Si_4)^{5+}$)			
		CASSCF		CASPT2		CASSCF		CASPT2	
	CFPs[a]	Re	Im	Re	Im	Re	Im	Re	Im
4f	B_0^2(ff)	760		1004		−1035		−990	
	B_1^2(ff)	−71	556	7	480	119	−37	209	206
	B_2^2(ff)	658	125	742	37	−339	270	−253	301
	B_0^4(ff)	1347		1166		435		478	
	B_1^4(ff)	1935	−789	2380	−728	609	−943	55	−678
	B_2^4(ff)	411	−133	257	140	−776	23	−524	−223
	B_3^4(ff)	−1032	−296	−875	−310	−811	536	−1146	348
	B_4^4(ff)	1686	−496	1825	−639	556	−880	316	−911
	B_0^6(ff)	167		−173		19		273	
	B_1^6(ff)	392	−56	520	−69	162	223	273	420
	B_2^6(ff)	659	−155	1143	−264	375	−123	374	−22
	B_3^6(ff)	755	7	998	−108	687	270	843	400
	B_4^6(ff)	−92	55	−176	317	92	42	−72	67
	B_5^6(ff)	41	599	−190	699	86	−537	313	−718
	B_6^6(ff)	16	−71	−31	−108	665	81	1481	−18
	sqrt(S_2)	649		717		544		541	
	sqrt(S_4)	1468		1603		941		852	
	sqrt(S_6)	492		717		485		796	
	S	969		1095		687		742	
5d	B_0^2(dd)	6476		6103		−9112		−8850	
	B_1^2(dd)	−1144	7073	−1149	6823	2560	−2276	2320	−2227
	B_2^2(dd)	5271	−655	4977	−588	−1590	300	−1387	214
	B_0^4(dd)	19811		19511		10103		9829	
	B_1^4(dd)	27459	−12471	27127	−12311	11644	−18518	11249	−18115
	B_2^4(dd)	11093	−1172	10874	−1023	−11199	3450	−11043	3209
	B_3^4(dd)	−16462	−6256	−16081	−6202	−10690	7831	−10510	7565
	B_4^4(dd)	25808	−7271	25118	−7160	6870	−16665	6728	−16522
	sqrt(S_2)	6341		6054		4727		4537	
	sqrt(S_4)	22407		21991		16106		15785	
	S	16466		16129		11869		11613	

[a]$B_{-q}^k = (-1)^q B_q^{k*}$, and hence only $q \geq 0$ parameters are thus given. $S = ({}^1/_3 \sum_{k=2,4,6} S_k)^{1/2}$ and $S = ({}^1/_2 \sum_{k=2,4} S_k)^{1/2}$ for 4f and 5d electrons of Ce^{3+} ion, respectively. $S_k = (1/(2k+1)) \sum_{q=-k}^{k} |B_q^k|^2)$.

the *ab initio* calculated energy levels. Comparing the CFPs obtained with CASSCF and CASPT2 level energies, we find that the second-order perturbation correction applied by CASPT2 to the energies strongly affects the magnitudes and

dx.doi.org/10.1021/jp5050207 | J. Phys. Chem. A 2014, 118, 4988−4994

signs of 4f CFPs, while its effects on 5d CFPs are minor. This arises from the fact that the energy correction is much smaller than the 5d energy-level splittings but is comparable to the 4f ones. The calculated CFPs for 4f and 5d electrons of Ce^{3+} may constitute a starting point for the CF analysis of energy levels of other lanthanide ions in X2-YSO, for which the *ab initio* calculations of energy levels are computationally formidable.

The **g**-factor tensors are very useful for the investigation of the EPR spectra of lanthanide ions in compounds.[9] Following the method described in section 2.4, the matrices $\mathbf{g}\cdot\mathbf{g}^{T}$ for the two types of Ce^{3+} in X2-YSO are obtained:

$$(\mathbf{g}\cdot\mathbf{g}^{T})_{Ce_{Y1}^{3+}} = \begin{pmatrix} 1.734 & -0.033 & 1.263 \\ -0.033 & 1.621 & 2.080 \\ 1.263 & 2.080 & 3.652 \end{pmatrix} \quad (8)$$

$$(\mathbf{g}\cdot\mathbf{g}^{T})_{Ce_{Y2}^{3+}} = \begin{pmatrix} 3.197 & 0.576 & -0.028 \\ 0.576 & 4.067 & -1.620 \\ -0.028 & -1.620 & 0.841 \end{pmatrix} \quad (9)$$

From the matrix $\mathbf{g}\cdot\mathbf{g}^{T}$, the **g**-tensors (in the diagonal form) for Ce^{3+} sites can be derived, as well as the direction cosines of the principal values of the **g**-tensors with respect to the chosen coordinate axes. Figure 2 plots the dependence of the calculated

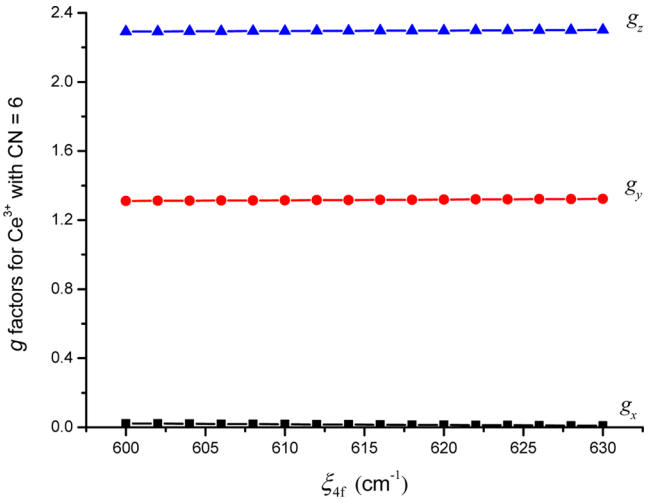

Figure 2. Calculated principal values of **g**-tensor as a function of the spin−orbit parameter of the 4f electron of Ce^{3+} ion occupying the Y1 site with CN = 6.

principal values on the magnitude of the spin−orbit interaction of the 4f electron of Ce^{3+} located at Y1 site (with CN = 6). It shows that the calculated **g** factors are almost invariant with respect to the change in the value of the 4f spin−orbit parameter, and hence the parameter value was kept fixed in the calculations of **g** factors. In Table 5, we list the calculated principal values of **g**-tensors for the two types of Ce^{3+} sites in X2-YSO, along with the experimental values from the Ce-doped LSO crystal[43] for comparison. One can see that the calculated values agree well with the experimental data. The predicted g_x values are small (0.015 and 0.394 for Ce^{3+} at Y1 and Y2 sites, respectively), while the g_z values are close to 2.300 (2.297 and 2.216 for Ce_{Y1}^{3+} and Ce_{Y2}^{3+} sites, respectively). Besides, the calculated g_x and g_y values for the Ce_{Y1}^{3+} site are much smaller than those for the Ce_{Y2}^{3+} site, but the g_z values for the two sites are similar.

Table 5. Calculated Principal Values of the g-Tensors for Ce^{3+} Ions in X2-YSO in Comparison with the Experimental Values for Ce^{3+} Ions in LSO

	site 1 (CN = 6)		site 2 (CN = 7)	
principal values	calcd	exptl[a]	calcd	exptl[a]
g_x	0.015	0	0.394	0.55
g_y	1.317	1.3	1.743	1.69
g_z	2.297	2.3	2.216	2.25

[a]Reference 43.

The 4f → 5d absorption spectrum of Ce-doped X2-YSO can be simulated by using the *ab initio* calculated 4f and 5d CFPs. A detailed description for the modeling of the intensity and bandwidth of the interconfigurational $4f^{N} \rightarrow 4f^{N-1}5d$ transitions of lanthanide ions doped in compounds can be found in refs 40, 46, and 47. The absorption spectra for the two types of Ce^{3+} in X2-YSO are calculated separately, and the results are plotted in Figure 3. Despite the site preference, the total absorption

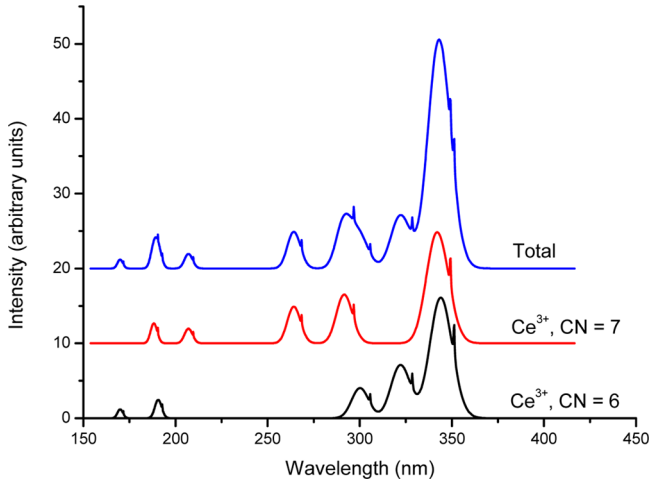

Figure 3. Calculated absorption spectra for Ce-doped X2-YSO. The values of the spin−orbit parameters from ref 40 (614.9 and 995.6 cm^{-1} for 4f and 5d electrons, respectively) are used for Ce^{3+} ions in X2-YSO, and the values of the parameter ΔE(fd) are taken from the energy differences between the centroids of the *ab initio* calculated 4f and 5d energy levels of Ce^{3+} ions in this work.

spectrum in the figure was obtained by a simple superposition of the simulated spectra of the two types of Ce^{3+} for a convenient comparison with experiments.

In order to distinguish the spectra for the two different types of Ce^{3+} in X2-YSO, the *ab initio* calculated energies and simulated absorption spectra are compared with experimental spectra for Ce-doped X2-YSO.[17,48] We first note by comparison that the lowest $4f_1 \rightarrow 5d_1$ transitions for both types of Ce^{3+} were not observed in the excitation spectra reported in ref 17, due to the limited wavelength range, while the excitation bands of the "Ce1" site at about 300 nm (33333 cm^{-1}), 260 nm (38462 cm^{-1}), 210 nm (47619 cm^{-1}), and 180 nm (55556 cm^{-1}) can be readily assigned to the $4f_1 \rightarrow 5d_{2-5}$ transitions of the seven-coordinated Ce_{Y2}^{3+}, respectively. The excitation bands at about 320 nm (31250 cm^{-1}) and 190 nm (52632 cm^{-1}) measured for the "Ce2" site can be ascribed to the $4f_1 \rightarrow 5d_{2,4}$ transitions of the six-coordinated Ce_{Y1}^{3+}, while the absence of the two other bands (i.e., the $4f_1 \rightarrow 5d_{3,5}$

dx.doi.org/10.1021/jp5050207 | J. Phys. Chem. A 2014, 118, 4988−4994

transitions) may be attributed to their overlap with the intense neighboring transition bands.

In the absorption spectra of Ce-doped X2-YSO measured by Kärner and co-workers (Figure 1a in ref 48), three absorption bands at about 354 nm (28229 cm^{-1}), 300 nm (33311 cm^{-1}), and 261 nm (38311 cm^{-1}) were observed. We assign these three bands to the lowest $4f_1 \rightarrow 5d_{1-3}$ transitions of the seven-coordinated Ce_{Y1}^{3+}, considering the good agreement between calculations and experiments. The lowest absorption band might also have some contribution from the lowest $4f_1 \rightarrow 5d_1$ transition of the six-coordinated Ce_{Y2}^{3+}, in view of the closeness in the calculated and experimental transition energies. Moreover, the calculated transition energies of Ce-doped X2-YSO are further compared with the $5d^1$ energy-level data obtained from experiments and *ab initio* calculations on Ce-doped LSO.[44] The X2-YSO and LSO crystals have similar crystal structures, and there is not much difference in the local structures of the dopant Ce^{3+}, which explains the good agreement between the $5d^1$ energy levels of Ce^{3+} in the two systems, as shown in Table 3.

4. CONCLUSIONS

Ab initio calculations have been performed in combination with phenomenological model analyses to study the structural and spectroscopic distinctions between the two types of Ce^{3+} located at the six-coordinated Y1 and seven-coordinated Y2 sites both with C_1 symmetry in X2-YSO. The DFT-PBE total energy calculations with the supercell approach show that the dopant Ce^{3+} prefers to occupy the Y2 site. Then, the CASSCF/CASPT2/RASSI-SO embedded cluster calculations were carried out to obtain the $4f^1$ and $5d^1$ energy levels and corresponding wave functions of Ce^{3+} at the Y1 and Y2 sites, from which the CFPs and anisotropic **g**-tensors of Ce^{3+} are extracted. The calculated **g**-tensors are in good agreement with the experimental data for Ce-doped LSO, which has a crystal structure similar to X2-YSO. On the basis of the comparisons between the calculations and experiments, the two types of Ce^{3+} centers observed in the experimental spectra are discriminated in association with the coordination structures of the dopant sites. The present theoretical approach can be conveniently utilized to investigate the structural and spectroscopic properties of Ce-doped luminescent materials, complementing the understanding of spectral properties observed in experiments. Moreover, the extractions of the CFPs and anisotropic **g**-tensors from *ab initio* calculations are very useful when Ce^{3+} occupies a low symmetry site, for which the spectral parameters can hardly be determined uniquely from both the least-squares fitting to the experimental spectra and the phenomenological model analyses.

AUTHOR INFORMATION

Corresponding Authors

*E-mail: wenjunkd@mail.ustc.edu.cn (J. Wen).

*E-mail: ninglx@mail.ahnu.edu.cn (L. X. Ning).

Notes

The authors declare no competing financial interest.

ACKNOWLEDGMENTS

This work was financially supported by the National Natural Science Foundation of China (Grant Nos. 11274299, 11174005, and 11374291).

REFERENCES

(1) Ricci, P. C.; Carbonaro, C. M.; Corpino, R.; Cannas, C.; Salis, M. Optical and Structural Characterization of Terbium-Doped Y_2SiO_5 Phosphor Particles. *J. Phys. Chem. C* **2011**, *115*, 16630−16636.

(2) Zhou, W.; Li, Y.; Zhang, R.; Wang, J.; Zou, R.; Liang, H. B. Ultraviolet to Near-Infrared Downconversion of Y_2SiO_5: Ce^{3+}, Yb^{3+} Nanobelt-Poly-EVA Films. *Opt. Lett.* **2012**, *37*, 4437−4439.

(3) Zhu, G.; Ci, Z. P.; Wang, Q.; Wen, Y.; Han, S. C.; Shi, Y. R.; Xin, S. Y.; Wang, Y. H. A New Type of Color Tunable Composite Phosphor Y_2SiO_5: Ce/$Y_3Al_5O_{12}$: Ce for Field Emission Displays. *J. Mater. Chem. C* **2013**, *1*, 4490−4496.

(4) Cates, S. L.; Cates, E. L.; Cho, M.; Kim, J. H. Synthesis and Characterization of Visible-to-UVC Upconversion Antimicrobial Ceramics. *Environ. Sci. Technol.* **2014**, *48*, 2290−2297.

(5) Sabooni, M.; Li, Q.; Kröll, S.; Ripp, L. Efficient Quantum Memory Using a Weakly Absorbing Sample. *Phys. Rev. Lett.* **2013**, *110*, No. 133604.

(6) Gündoğan, M.; Mazzera, M.; Ledingham, P. M.; Cristiani, M.; de Riedmatten, H. Coherent Storage of Temporally Multimode Light Using a Spin-Wave Atomic Frequency Comb Memory. *New J. Phys.* **2013**, *15*, No. 045012.

(7) Leibrandt, D. R.; Thorpe, M. J.; Chou, C. W.; Fortier, T. M.; Diddams, S. A.; Rosenband, T. Absolute and Relative Stability of an Optical Frequency Reference Based on Spectral Hole Burning in Eu^{3+}: Y_2SiO_5. *Phys. Rev. Lett.* **2013**, *111*, No. 237402.

(8) Thorpe, M. J.; Rippe, L.; Fortier, T. M.; Kirchner, M. S.; Rosenband, T. Frequency Stabilization to 6×10^{-16} via Spectral-Hole Burning. *Nat. Photonics* **2011**, *5*, 688−693.

(9) Guillot-Noël, O.; Goldner, P.; Le Du, Y.; Baldit, E.; Monnier, P.; Bencheikh, K. Hyperfine Interaction of Er^{3+} Ions in Y_2SiO_5: An Electron Paramagnetic Resonance Spectroscopy Study. *Phys. Rev. B* **2006**, *74*, No. 214409.

(10) Lauritzen, B.; Timoney, N.; Gisin, N.; Afzelius, M.; de Riedmatten, H.; Sun, Y.; Macfarlane, R. M.; Cone, R. L. Spectroscopic Investigations of Eu^{3+}:Y_2SiO_5 for Quantum Memory Applications. *Phys. Rev. B* **2012**, *85*, No. 115111.

(11) Yan, Y.; Karlsson, J.; Rippe, L.; Walther, A.; Serrano, D.; Lindgren, D.; Pistol, M.; Kröll, S.; Goldner, P.; Zheng, L.; Xu, J. Measurement of Linewidths and Permanent Electric Dipole Moment Change of the Ce 4f-5d Transition in Y_2SiO_5 for Qubit Readout Scheme in Rare-Earth Ion Based Quantum Computing. *Phys. Rev. B* **2013**, *87*, No. 184205.

(12) Serrano, D.; Yan, Y.; Karlsson, J.; Rippe, L.; Walther, A.; Kröll, S.; Ferrier, A.; Goldner, P. Impact of the Ion−Ion Energy Transfer on Quantum Computing Schemes in Rare-Earth Doped Solids. *J. Lumin.* **2014**, *151*, 93−99.

(13) Jia, Y. C.; Huang, Y. J.; Zheng, Y. H.; Guo, N.; Qiao, H.; Zhao, Q.; Lv, W. Z.; You, H. P. Color Point Tuning of $Y_3Al_5O_{12}$: Ce^{3+} Phosphor via Mn^{2+}−Si^{4+} Incorporation for White Light Generation. *J. Mater. Chem.* **2012**, *22*, 15146−15152.

(14) Shi, Y. R.; Wang, Y. H.; Wen, Y.; Zhao, Z. Y.; Liu, B. T.; Yang, Z. G. Tunable Luminescence $Y_3Al_5O_{12}$: 0.06Ce^{3+}, xMn^{2+} Phosphors with Different Charge Compensators for Warm White Light Emitting Diodes. *Opt. Express* **2012**, *20*, 21656−21664.

(15) Setlur, A. A.; Heward, W. J.; Hannah, M. E.; Happek, U. Incorporation of Si^{4+}−N^{3-} into Ce^{3+} -Doped Garnets for Warm White LED Phosphors. *Chem. Mater.* **2008**, *20*, 6277−6283.

(16) Lin, J.; Su, Q.; Zhang, H.; Wang, S. Crystal Structure Dependence of the Luminescence of Rare Earth Ions (Ce^{3+}, Tb^{3+}, Sm^{3+}) in Y_2SiO_5. *Mater. Res. Bull.* **1996**, *31*, 189−196.

(17) Drozdowski, W.; Wojtowicz, A. J.; Wiśniewski, D.; Szupryczyński, P.; Janus, S.; Lefaucheur, J. L.; Gou, Z. VUV Spectroscopy and Low Temperature Thermoluminescence of LSO: Ce and YSO: Ce. *J. Alloys Compd.* **2004**, *380*, 146−150.

(18) Reid, M. F.; Duan, C. K.; Zhou, H. W. Crystal-Field Parameters from Ab Initio Calculations. *J. Alloys Compd.* **2009**, *488*, 591−594.

(19) Hu, L.; Reid, M. F.; Duan, C. K.; Xia, S.; Yin, M. Extraction of Crystal-Field Parameters for Lanthanide Ions from Quantum-Chemical Calculations. *J. Phys.: Condens. Matter* **2011**, *23*, No. 045501.

(20) Wen, J.; Ning, L. X.; Duan, C. K.; Chen, Y.; Zhang, Y.; Yin, M. A Theoretical Study on the Structural and Energy Spectral Properties of Ce^{3+} Ions Doped in Various Fluoride Compounds. *J. Phys. Chem. C* **2012**, *116*, 20513−20521.
(21) Wen, J.; Reid, M. F.; Ning, L. X.; Zhang, J.; Zhang, Y. F.; Duan, C. K.; Yin, M. Ab-Initio Calculations of Judd−Ofelt Intensity Parameters for Transitions between Crystal-Field Levels. *J. Lumin.* **2014**, *152*, 54−57.
(22) Perdew, P.; Burke, K.; Ernzerhof, M. Generalized Gradient Approximation Made Simple. *Phys. Rev. Lett.* **1996**, *77*, 3865−3868.
(23) Kresse, G.; Furthmüller, J. Efficient Iterative Schemes for Ab Initio Total-Energy Calculations Using a Plane-Wave Basis Set. *Phys. Rev. B* **1996**, *54*, 11169−11186.
(24) Kresse, G.; Joubert, D. From Ultrasoft Pseudopotentials to the Projector Augmented-Wave Method. *Phys. Rev. B* **1999**, *59*, 1758−1775.
(25) Blöchl, P. E. Projector Augmented-Wave Method. *Phys. Rev. B* **1994**, *50*, 17953−17979.
(26) Barandiarán, Z.; Seijo, L. The Abinitio Model Potential Representation of the Crystalline Environment. Theoretical Study of the Local Distortion on NaCl: Cu^{+}. *J. Chem. Phys.* **1988**, *89*, 5739−5746.
(27) Roos, B. O.; Taylor, P. R.; Siegbahn, P. E. M. A Complete Active Space SCF method (CASSCF) Using a Density-Matrix Formulated Super-CI Approach. *Chem. Phys.* **1980**, *48*, 157−173.
(28) Siegbahn, P. E. M.; Heiberg, A.; Almlöf, J.; Roos, B. O. The Complete Active Space SCF (CASSCF) Method in a Newton-Raphson Formulation with Application to the HNO Molecule. *J. Chem. Phys.* **1981**, *74*, 2384−2396.
(29) Andersson, K.; Malmqvist, P.-Å.; Roos, B. O.; Sadlej, A. J.; Wolinski, K. Second-Order Perturbation Theory with a CASSCF Reference Function. *J. Phys. Chem.* **1990**, *94*, 5483−5488.
(30) Andersson, K.; Malmqvist, P.-Å.; Roos, B. O. Second-Order Perturbation Theory with a Complete Active Space Self-Consistent Field Reference Function. *J. Chem. Phys.* **1992**, *96*, 1218−1226.
(31) Zaitsevskii, A.; Malrieu, J. P. Multi-Partitioning Quasidegenerate Perturbation Theory. A New Approach to Multireference Moller-Plesset Perturbation Theory. *Chem. Phys. Lett.* **1995**, *233*, 597−604.
(32) Finley, J.; Malmqvist, P.-Å.; Roos, B. O.; Serrano-Andrés, L. The Multi-State CASPT2Method. *Chem. Phys. Lett.* **1998**, *288*, 299−306.
(33) Karlström, G.; Lindh, R.; Malmqvist, P.; Roos, B. O.; Ryde, U.; Veryazov, V.; Widmark, P.; Cossi, M.; Schimmelpfennig, B.; Neograd, P.; Seijo, L. Molcas: A Program Package for Computational Chemistry. *Comput. Mater. Sci.* **2003**, *28*, 222−239.
(34) Malmqvist, P.-Å.; Roos, B. O.; Schimmelpfennig, B. The Restricted Active Space (RAS) State Interaction Approach with Spin-Orbit Coupling. *Chem. Phys. Lett.* **2002**, *357*, 230−240.
(35) Seijo, L.; Barandiaran, Z.; Ordejon, B. Transferability of Core Potentials to f and d States of Lanthanide and Actinide Ions. *Mol. Phys.* **2003**, *101*, 73−80.
(36) Barandiaran, Z.; Seijo, L. The Abinitio Model Potential Method. Cowan−Griffin Relativistic Core Potentials and Valence Basis Sets from Li (Z = 3) to La (Z = 57). *Can. J. Chem.* **1992**, *70*, 409−415.
(37) Görller-Walrand, C.; Binnemans, K. *Handbook on the Physics and Chemistry of Rare Earths*; Gschneidner, K. A., Jr., Eyring, L., Eds.; Elsevier Science B. V.: Amsterdam, 1996; Vol. *23*, pp 121−283.
(38) Liu, H. G.; Yang, M.; Zheng, W. C. Link between EPR g-Factors and Local Structure of the Orthorhombic Ce^{3+} Center in $Y_3Al_5O_{12}$ and $Lu_3Al_5O_{12}$ Garnets. *Chem. Phys. Lett.* **2012**, *554*, 214−218.
(39) Weil, J. A.; Bolton, J. R. *Electron Paramagnetic Resonance: Elementary Theory and Practical Applications*; Wiley: Hoboken, NJ, 2007; Chapter 4, pp 85−111.
(40) van Pieterson, L.; Reid, M. F.; Wegh, R. T.; Soverna, S.; Meijerink, A. $4f^n \rightarrow 4f^{n-1}5d$ Transitions of the Light Lanthanides: Experiment and Theory. *Phys. Rev. B* **2002**, *65*, No. 045113.
(41) Maksimov, B. A.; Ilyukhin, V. V.; Kharitonov, Y. A.; Belov, N. V. Crystal Structure of Yttrium Oxyorthosilicate $Y_2O_3SiO_2$ and Y_2SiO_5. *Kristallografiya* **1970**, *15*, 926−933.
(42) Shannon, R. D. Revised Effective Ionic Radii and Systematic Studies of Interatomic Distances in Halides and Chalcogenides. *Acta Crystallogr.* **1976**, *A32*, 751−767.
(43) Pidol, L.; Guillot-Noël, O.; Kahn-Harari, A.; Viana, B.; Pelenc, D.; Gourier, D. EPR Study of Ce^{3+} Ions in Lutetium Silicate Scintillators $Lu_2Si_2O_7$ and Lu_2SiO_5. *J. Phys. Chem. Solids* **2006**, *67*, 643−650.
(44) Ning, L. X.; Lin, L. H.; Li, L. L.; Wu, C. B.; Duan, C. K.; Zhang, Y. F.; Seijo, L. Electronic Properties and 4f → 5d Transitions in Ce-Doped Lu_2SiO_5: A Theoretical Investigation. *J. Mater. Chem.* **2012**, *22*, 13723−13731.
(45) Dorenbos, P. 5d-Level Energies of Ce^{3+} and the Crystalline Environment. I. Fluoride Compounds. *Phys. Rev. B* **2000**, *62*, 15640−15649.
(46) Ma, C. G.; Trevisani, M.; Piccinelli, F.; Ivanovskikh, K. V.; Bettinelli, M.; Brik, M. G. Analysis of Vacuum Ultraviolet Electronic Spectra of Ce^{3+} and Pr^{3+} Ions in $Ca_9Lu(PO_4)_7$: Crystal-Field Calculations and Simulation of Optical Spectra. *J. Phys.: Condens. Matter* **2013**, *25*, No. 165503.
(47) van Pieterson, L.; Reid, M. F.; Burdick, G. W.; Meijerink, A. $4f^n \rightarrow 4f^{n-1}5d$ Transitions of the Heavy Lanthanides: Experiment and Theory. *Phys. Rev. B* **2002**, *65*, No. 045114.
(48) Karner, T.; Laguta, V. V.; Nikl, M.; Shalapska, T.; Zazubovich, S. On the Origin of Cerium-Related Centres in Lead-Containing Single Crystalline Films of Y_2SiO_5: Ce and Lu_2SiO_5: Ce. *J. Phys. D: Appl. Phys.* **2014**, *47*, No. 065303.